Adaptive droop control strategy for Flywheel Energy Storage Systems: A Power Hardware-in-the-Loop validation☆

Shahab Karrari *, Giovanni De Carne, Mathias Noe

Institute for Technical Physics (ITEP), Karlsruhe Institute of Technology (KIT), Eggenstein-Leopoldshafen, Germany

ARTICLE INFO

ABSTRACT

Low-inertia power systems can suffer from high rates of change of frequency during imbalances between the generation and the demand. Fast-reacting storage systems such as a Flywheel Energy Storage System (FESS) can help maintain the frequency by quickly reacting to frequency disturbances, with no concern over its lifetime. While a modern high-speed FESS has a significantly higher energy density than the conventional low-speed ones, the capacity of this storage technology is still limited. Therefore, this paper proposes a new adaptive droop controller for a FESS, considering the practical advantages and also limitations of this storage technology. The proposed controller increases the contribution of the FESS for frequency support during the first instances of a disturbance, while it reduces its output when the frequency is recovering. To verify the advantages of the proposed control strategy, the controller is implemented on a real 60 kW high-speed FESS using the concept of rapid control prototyping. Next, the performance of the FESS with the new controller is tested using Power Hardware-in-the-Loop simulations in a low-voltage microgrid. The PHIL simulation results show that the proposed adaptive controller improves the performance of the FESS in terms of limiting the frequency deviations, while preserving more energy in the FESS.

1. Introduction

With the decreasing system inertia in power systems around the globe, the rate of change of frequency during disturbances is steadily increasing [1,2], reducing the time available for reacting to frequency deviations. Therefore, there is a greater need for fast-reacting active grid components, such as a Flywheel Energy Storage System (FESS), which can rapidly inject or absorb high amounts of active power, when necessary [3]. However, the energy content of a FESS is rather limited, in comparison to Li-ion batteries, even in a modern high-speed FESS. Therefore, it is important to use the stored energy in a FESS in an optimal way, while effectively responding to frequency deviations.

Droop control is most commonly used for determining the contribution of energy storage systems during frequency deviations, similar to conventional generation units. However, energy storage systems have several important limitations, such as the available energy at each moment and their lifetime, which should be considered when providing frequency support services. With the aim of considering these limitations, there have been several adaptive droop control designs suggested

in literature for Li-ion batteries, including in [4–9]. These adaptive controllers often aim to maintain the battery's State of Charge (SOC) in a specific range, avoiding low and high SOC values (deep discharging and overcharging), in order to maintain its effective lifetime. For instance, authors in [8] and [9] propose nonlinear functions for increasing the droop coefficient for high SOC values while discharging, and reducing it at low values of SOC. Nevertheless, these control strategies cannot necessarily be applied to a FESS, due to its different requirements and charging and discharging characteristics of this storage technology, and the fact that there are no SOC limits or lifetime concerns in a FESS. However, below a certain SOC (often below 25% [10]), the maximum power of the FESS becomes limited, due to the torque limit of the electrical machine, and depends on its instantaneous rotational speed. Moreover, as discussed, a FESS has significantly less energy density and shorter discharge times, in comparison to the Li-ion batteries. Therefore, there is a clear need to propose an adaptive droop control strategy, specifically designed for a FESS, which takes into account the specific requirements of this storage technology. However, to our knowledge, such a controller has not yet been proposed in literature. In [11], a

---

novel adaptive frequency and voltage controller has been proposed for a FESS, with the aim of coordinating the provided frequency and voltage support, due to the resistive nature of low-voltage grids and microgrids. But this controller does not include the practical limitations of a real FESS into the control structure. In addition, to our knowledge, no experimental validation of adaptive droop controllers using a real FESS has been reported in literature. The experiments presented in [11] use a constant DC power supply to represent the flywheel and its converter, which clearly cannot reflect the practical limitations of this storage technology.

In this paper, an adaptive droop controller for a high-speed FESS is proposed, which takes into account the severity of the frequency deviation, the instantaneous rotational speed of the FESS, and the power limitation of the FESS at low speeds. In the proposed design, following a frequency disturbance, the droop coefficient increases with the amplitude and the derivative of the frequency deviation, in order to maximize the frequency support provided by the FESS during the first seconds of the frequency deviations. However, after passing the frequency nadir, the droop coefficient is reduced, in order to slow down reaching the maximum or minimum rotational speeds of the FESS. For validating the performance of the proposed control strategy, the controller is implemented on a real 60 kW commercial high-speed FESS, as an external control layer, using the concept of rapid control prototyping, where the proposed controller is simulated in real time, while being tested on the real hardware. Next, the high-speed FESS equipped with the new adaptive droop controller, is tested in a microgrid by means of Power Hardware-in-the-Loop (PHIL) evaluation in two different scenarios.

The remaining of this paper is organized as follows. The structure of the proposed controller is described in Section 2. The experimental validation of the proposed control strategy is presented in Section 3, followed by the conclusions given in Section 4.

2. The proposed adaptive droop control

In a conventional droop controller, the droop coefficient (D) is always constant and independent of the severity of the frequency disturbance. It determines the required change in the active power (ΔP) with respect to changes in the grid frequency (Δf) using a linear relationship, in which

$$\Delta P = D \Delta f. \tag{1}$$

Nevertheless, the droop coefficient is a control parameter, and it can be altered in real-time, according to the grid frequency, and in the case of energy storage systems, according to the available energy, as suggested in [4–9] for batteries.

In this paper, an interval-based approach is proposed, similar to [12], in which the period of a frequency disturbance is divided into two different intervals, A and B, according to the sign of $\Delta f \frac{d\Delta f}{dt}$. These intervals are depicted in Fig. 1. For each interval, a different droop coefficient is applied, which is described in detail in the following subsections.

2.1. Interval A: Deviating from the steady-state frequency

A FESS is a short-term energy storage technology with high power capabilities, which can rapidly provide or absorb power with high ramp rates, and almost no effects on its lifetime or effective capacity. To take advantage of these characteristics of the FESS for frequency support, in this paper, it is suggested to rapidly increase the droop coefficient following a frequency disturbance, with respect to the severity of the frequency deviation and its time derivative, which is expressed mathematically in (2). According to (2), as soon as the frequency begins to deviate from its steady-state and before reaching the frequency nadir, i.e., $\Delta f \frac{d\Delta f}{dt} > \epsilon$, the droop coefficient increases linearly with the frequency error ($D_1|\Delta f|$) and the rate of change of frequency ($D_2|\frac{d\Delta f}{dt}|$),
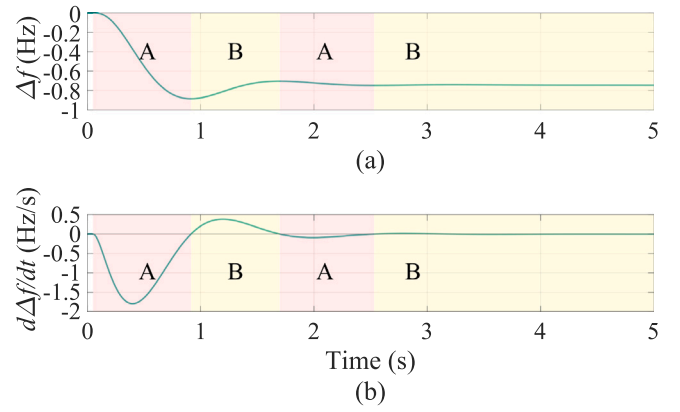

Fig. 1. Separating the period of a frequency disturbance into two different intervals, A and B, according to the sign of $\Delta f \frac{d\Delta f}{dt}$. (a) Frequency deviation Δf, (b) time derivative of the frequency deviation $\frac{d\Delta f}{dt}$.

Table 1
The parameters for the proposed adaptive droop controller.

Parameter	Value	Parameter	Value
D_0	40 p.u.	D_1	500 p.u.
D_4	25 p.u.	D_2	500 p.u.
$D_{3\max}$	1	ϵ	3×10^{-6}

from the initial value of D_0. Therefore, the proposed controller increases the contribution of the FESS by increasing the droop coefficient with respect to the severity of the frequency deviation, in particular during the first instances of a frequency disturbance, where a high rate of change of frequency followed by a high frequency error is expected (interval A). Moreover, with the addition of the time derivative of the frequency in the proposed controller, the FESS provides a virtual inertia response, similar to synchronous generators, taking into account the minor measurement and control delays in the FESS.

$$D = \begin{cases} D_0 + D_1|\Delta f| + D_2|\frac{d\Delta f}{dt}| & \text{, if } \Delta f \frac{d\Delta f}{dt} > \epsilon \\ D_3(\omega_m)D_4 & \text{, if } \Delta f \frac{d\Delta f}{dt} \leq -\epsilon \end{cases} \tag{2}$$

In (2), D_0, D_1, D_2, D_4 are constant parameters with their values given in Table 1, while D_3 is a function of the rotational speed of the flywheel with the maximum value of $D_{3\max}$, which is explained later in Section 2.2. To avoid a continuous change within the two states in (2), a small value of ϵ is used rather than zero in this paper, which should be higher than the expected level of noise in the frequency measurements.

As seen in (2), the proposed adaptive droop controller requires an estimate of the time derivative of the frequency. However, it has been shown that applying a differential operator on the frequency signal can lead to noise amplification, unrealistically high values, and stability issues [13]. Therefore, in this paper, we use the Dual Second Order Generalized Integrator Frequency-Locked Loop (DSOGI-FLL) [14], which can generate the frequency derivative signal without using the differential operator, avoiding the aforementioned issues. The parameters of the DSOGI-FLL are chosen according to [14]. Moreover, as shown in [14], the dynamics of the DSOGI-FLL are in the range of 50 to 150 ms, depending on the used parameters, which is significantly less than the frequency dynamics of the microgrid, which are in the second region.

2.2. Interval B: Recovering towards the steady-state value

In the proposed control design, whenever the frequency is deviating away from its steady-state value (interval A), no energy-related limit is applied in the control structure, in order to fully benefit from the

high power capabilities of the FESS for supporting the grid frequency, in particular during the first instances of a frequency disturbance. The only limitation in this period is the torque limit of the electrical machine, which limits the active power in low rotational speeds (see the dashed red line in Fig. 2). This is due to the fact that, at low speeds, a higher electrical torque is required to deliver the nominal power, which can be higher than the electrical machine's maximum torque. The speed after which the nominal power can be provided is often chosen to be half of the maximum rational speed, since in comparison to a fully charged FESS, doubling the electrical torque is necessary to provide the same power [10]. But whenever the frequency has passed its minimum or maximum point (frequency nadir), recovering towards its steady-state value, or the frequency has already settled down, it is important to limit the contribution of the FESS, considering its limited energy content. In such periods, other storage technologies such as Li-ion batteries or diesel generators should compensate for the power imbalance, which can contribute in a longer period. While a modern high-speed FESS has significantly higher capacity in comparison to the conventional low-speed FESS, due to the use of active magnetic bearings and vacuum enclosures [10], its capacity is still significantly lower than what Li-ion batteries can offer.

Therefore, in the proposed control design, after the passing the frequency nadir and when the frequency is returning to its new steady-state value (or it has already settled down), a smaller droop coefficient D_4 is applied, which is also scaled down using the scaling factor $D_3(\omega_m)$. This is a necessary step when using a real FESS, considering its low energy content, its self-discharge rate, and its power limitations in low rotational speeds, as the droop coefficient in this period determines the charging/discharging rate of the FESS over a longer period of time.

The scaling factor $D_3(\omega_m)$ is expressed mathematically in (3) and illustrated in Fig. 2. As seen, $D_3(\omega_m)$ is a piecewise function of the rotational speed of the flywheel, and also depends on the sign of the frequency deviations, which determines the direction of the power flow. By assuming the machine torque limitations starts when the speed falls below half of the maximum rotational speed [10], which corresponds to an SOC of 25%, then the SOC of 75% would be the center of the range, in which the FESS has its full power capability. The SOC of 75% corresponds to the speed of 0.866 p.u. in a FESS, which is represented by ω_k in (3). As shown in (3), whenever this point is surpassed, and the frequency deviation is positive, i.e., the FESS is being charged, the droop coefficient is reduced linearly until reaching zero at the maximum rotational speed (the blue line in Fig. 2). This helps slow down reaching the maximum speed of the FESS, after which the FESS will no longer be available for providing the frequency support services during over-frequency incidents. Below the rotational speed of ω_k (0.866 p.u.), the droop coefficient is only reduced when the speed is below 0.5 p.u., which is due to the torque limit of the electrical machine of the FESS. Similarly, whenever the speed of the FESS falls below the ω_k threshold and the frequency deviation is negative, i.e., the FESS is being discharged, the discharging rate is reduced linearly until reaching zero, when the FESS is fully empty (the yellow line in Fig. 2). This helps to reduce the rate at which the FESS is being emptied, prolonging the time that the FESS is available for providing frequency support services during under-frequency events. Whenever the speed of the FESS is higher than ω_k and the FESS is being discharged (under-frequency events), or the speed is below ω_k and the FESS is being charged (over-frequency events), no limit on the FESS is applied and the scaling factor D_3 equals to 1, as shown in (3).

$$D_3(\omega_m) = \begin{cases} 1 & , \text{if } \omega_m > \omega_k \ \& \ \Delta f \leq 0 \\ \frac{1}{1-\omega_k}(1-\omega_m) & , \text{if } \omega_m > \omega_k \ \& \ \Delta f > 0 \\ \frac{1}{\omega_k}\omega_m & , \text{if } \omega_m \leq \omega_k \ \& \ \Delta f \leq 0 \\ 1 & , \text{if } \omega_m \leq \omega_k \ \& \ \Delta f > 0 \end{cases} \qquad (3)$$

Using the proposed controller can potentially extend the time, in which the FESS will be available for providing the frequency support services, by reducing the charging and discharging rate near the limits of the FESS. This is shown experimentally in the following section.
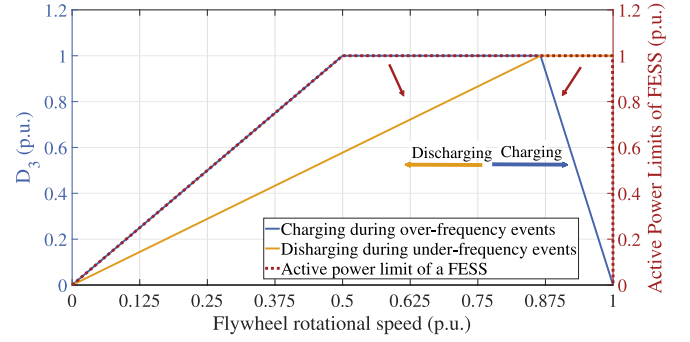

Fig. 2. The scaling of the droop coefficient as a function of its rotational speed, $D_3(\omega_m)$, when the frequency is recovering towards a new stead-state value. The dashed red line shows the active power limitation of a FESS in per unit.
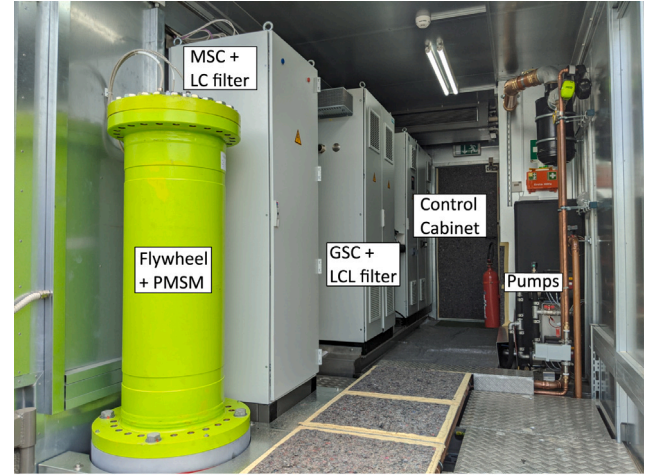

Fig. 3. Inside view of the container holding the 60 kW high-speed FESS with all its main and auxiliary components.

3. Rapid control prototyping and Power Hardware-in-the-Loop experimental validation

To experimentally validate the performance of the proposed adaptive droop control strategy, the controller is implemented on a real commercial 60 kW high-speed FESS, shown in Fig. 3, using the concept of rapid control prototyping, as a secondary controller. A schematic diagram of the established setup for validating the performance of the proposed control design is shown in Fig. 4. As seen in Fig. 4, the proposed controller is simulated in real-time on an Opal-RT OP5700 real-time simulator. Within the real-time simulator, the controller receives the grid voltages at the point of common coupling, and measures the frequency and its derivative using the DSOGI-FLL [14], and generates the active power reference for the FESS. The active power reference is then sent to the real FESS using one of the analog outputs of the real-time simulator. This concept in which a new controller is simulated in real-time while being tested on the real hardware is known as rapid control prototyping [15]. Since the proposed controller also requires the SOC or the speed of the FESS, the SOC of the FESS, which is measured internally in the FESS controller, is sent to the real-time simulator using an Ethernet connection and the Modbus TCP/IP protocol from the industrial controller of the FESS. A separate CPU core of the real-time simulator is dedicated for handling the communication between the industrial controller of the FESS and the real-time simulator. This Ethernet connection can also be used to send reference commands, such as the active power reference, to the FESS. However, since the Modbus protocol is slow and non-deterministic by nature [16], the faster analog
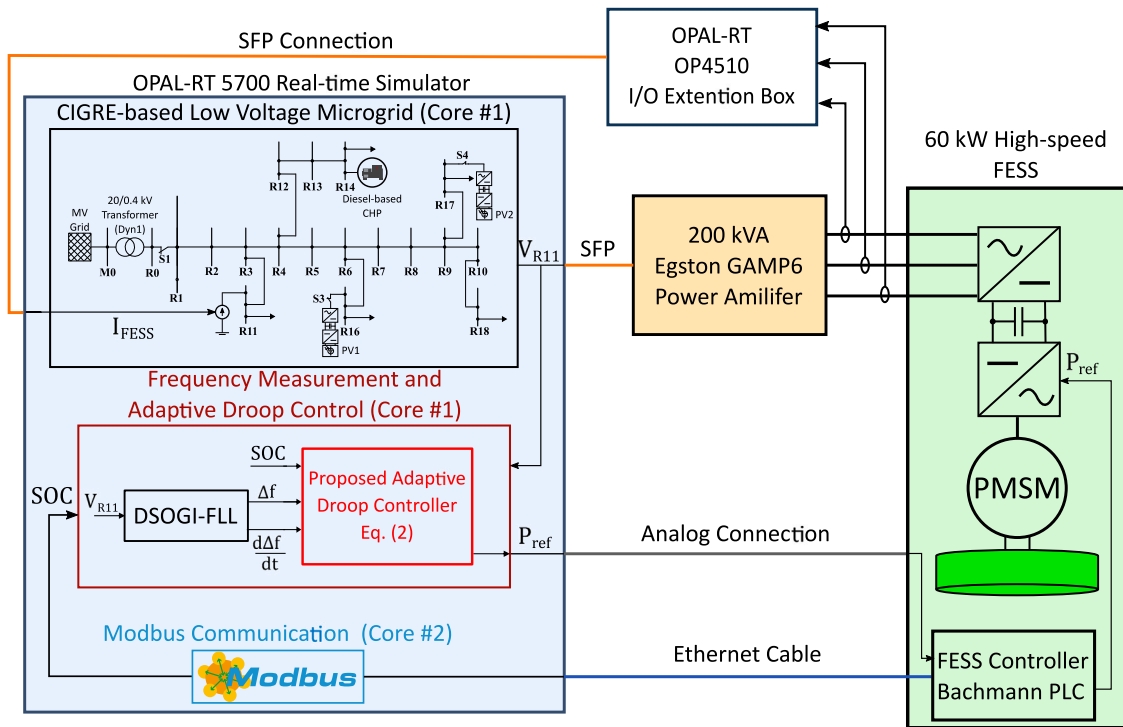
Fig. 4. The setup for rapid control prototyping of the proposed controller and PHIL simulation of the 60 kW high-speed FESS.
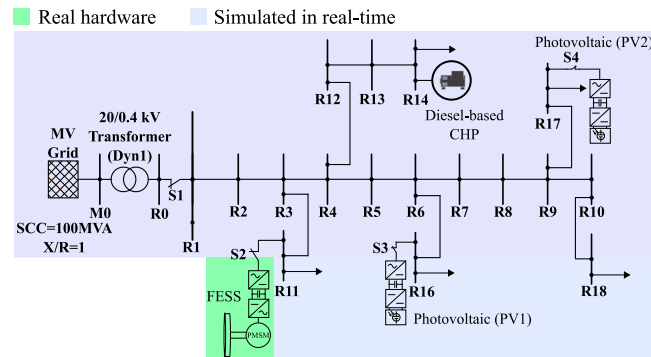

Fig. 5. The single-line diagram of the studied low voltage microgrid, which is based on the CIGRÉ European low voltage network benchmark [18].

signal transmission (a 4–20 mA current signal) is preferred in this work for sending the active power reference to the FESS. A more detailed description of the setup, the high-speed FESS and a validated model of the FESS can be found in [17].

For testing the FESS equipped the new controller in a realistic grid scenario, a low-voltage microgrid (see Fig. 5), based on the CIGRÉ European low voltage network benchmarked [18] is simulated in real-time. The single-line diagram of the studied microgrid is depicted in Fig. 5, in which two PV systems, a combined heat and power (CHP) system, and a high-speed FESS is added to allow an autonomous operation of the microgrid. The parameters of the distributed energy resources added to the CIGRÉ European low voltage network benchmark, including the FESS, can be found in [17] and [19]. The CIGRÉ-based low-voltage microgrid in also simulated in real-time on the Opal-RT's OP5700 real-time simulator, with the simulation time steps of only 24 μs. This relatively low simulation time step is achieved using the state-space nodal solver [20] and selecting bus R4 (see Fig. 5) as the decoupling point of system equations.

The FESS equipped with the proposed controller is tested in the microgrid by means of the Power Hardware-in-the-Loop (PHIL) simulations [21]. As shown in Fig. 4, the simulated grid voltages at the terminals of the FESS (bus R11) are sent to a 200 kVA switch-mode power amplifier from EGSTON Power Electronics using a Small-Factor pluggable (SFP) connection and Xilinx's Aurora protocol. The power amplifier can feed power and absorb power from the FESS. The currents of the FESS are measured at the connection point to the FESS using the DQ640ID-B Danisense current transformers and send to an Opal-RT OP4510 I/O extension box, which sends the measured values using another SFP connection to the real-time simulator in order to close the loop. The ideal transformer method is used for interfacing the FESS and the real-time simulation, as it is the most simple and common interfacing algorithm for PHIL simulations in practice [22]. While the voltages at the FESS terminal are also measured and sent back to the real-time simulator, they are only used for calculating the FESS power within the simulator and are not used in the PHIL interfacing algorithm.

For comparison purposes, four different cases have been studied in each test scenario:

- **Case I**: No FESS.
- **Case II**: FESS with a constant droop coefficient of D_0.
- **Case III**: FESS with the adaptive droop controller proposed in [9] with exponent component (n) of 2.
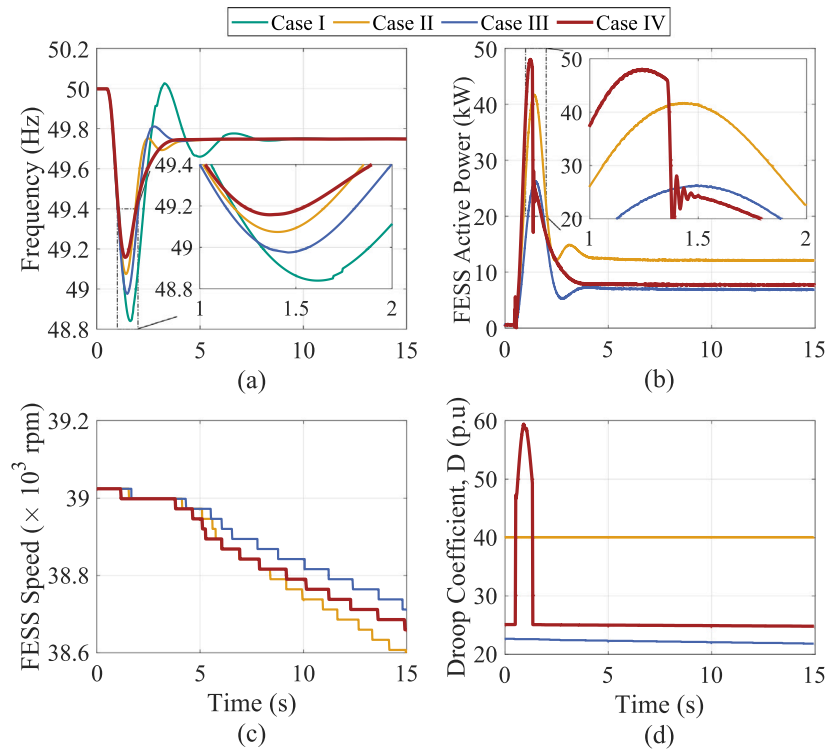
Fig. 6. The results of rapid control prototyping and PHIL simulations in scenario A, the microgrid islanding. (a) The frequency, (b) the measured active power of the FESS, (c) the rotational speed of the FESS, received using the Ethernet connection and the Modbus protocol (high latency can be observed), and (d) the variations of the droop coefficient.

• **Case IV**: FESS with the proposed adaptive droop controller, as described in Section 2.

In the following, the behavior of the microgrid in these four cases is investigated in two different scenarios, in order to evaluate the performance of the proposed controller in both short-term and long-lasting frequency deviations.

3.1. Scenario A: Islanding of the microgrid

The scenario includes the sudden islanding of the microgrid by opening of the circuit breaker S1, while the microgrid is absorbing 80 kW of power from the medium voltage grid. This should lead to a significant change in the microgrid frequency, as the synchronous generator of the CHP system is the only source of inertia in the system. Before conducing each experiment, the FESS is charged to reach the SOC of 75%, which corresponds to a rotational speed of approximately 38,971 rpm for this particular FESS (maximum speed: 45,000 rpm). The two PV systems cannot participate in the frequency regulation, as they are operating at their maximum power point.

The results of the rapid control prototyping and PHIL simulations of the 60 kW FESS for all studied cases in this scenario are shown in Fig. 6. It can be seen from Fig. 6(a) that using the proposed controller, presented as case IV, leads to the best results in terms of minimizing the maximum frequency deviation, and the most improved frequency nadir is achieved using this controller. This is achieved by a faster and higher injection of active power, in comparison to the other controllers, as shown in Fig. 6(b). But since the active power is reduced after passing the frequency nadir, the FESS has more energy at the end of the disturbance using the proposed controller, in comparison to the constant droop controller of case II, while performing better in terms of providing the frequency support. It can be observed from Fig. 6(c) that the speed of the FESS at the end of the disturbance is higher using the proposed controller, in comparison to case II. It is clear that the adaptive droop controller of Case III is more successful in

maintaining the energy of the FESS, as shown in Fig. 6(c). However, it can be seen from Fig. 6(a) that this controller performs even worse than the conventional droop control in terms of minimizing the maximum frequency deviation, which jeopardizes the advantages of using the energy storage system for frequency support applications. It should also be noted that the speed of FESS shown in Fig. 6(c) show discretization and a large latency, since these values are read from the internal controller of the FESS using the Modbus TCP/IP protocol, which is known to be slow with show high latencies [16]. Lastly, Fig. 6(d) shows the changes in the droop coefficient in each case. It can be seen that the increase in the droop coefficient in the proposed control design only occurs at the first instances of the frequency deviation until reaching the frequency nadir, which leads to the improved performance of the FESS in terms of minimizing the frequency deviation, while preserving the energy content of the FESS.

3.2. Scenario B: Long-term operation of the microgrid with intermittent generation

In order to observe the effect of the droop scaling factor $D_3(\omega_m)$ in the proposed control design, the FESS is tested in another scenario, which lasts a longer period of time. For this scenario, the two PV systems follow the measured power profile of an actual PV system at a low voltage distribution grid in southern Germany in June 2018 [23]. The recorded PV power has been scaled accordingly and given as the output of the two PV system of the microgrid. The measured power profile is loaded on the real-time target, before running the simulations. The microgrid is again islanded and then continues to operate in the autonomous mode of operation at an off-nominal frequency, with the PV system fluctuating their outputs according to the measurement data. These active power changes of the PV systems lead to slight changes in the microgrid frequency. The FESS attempts to limit these frequency deviations by quickly reacting to these changes. Similar to the previous scenario, the FESS is charged up to 75% of SOC, before running the experiments. The experiments in each case are continued until the FESS reaches an SOC of zero (standstill), depending on the applied controller.
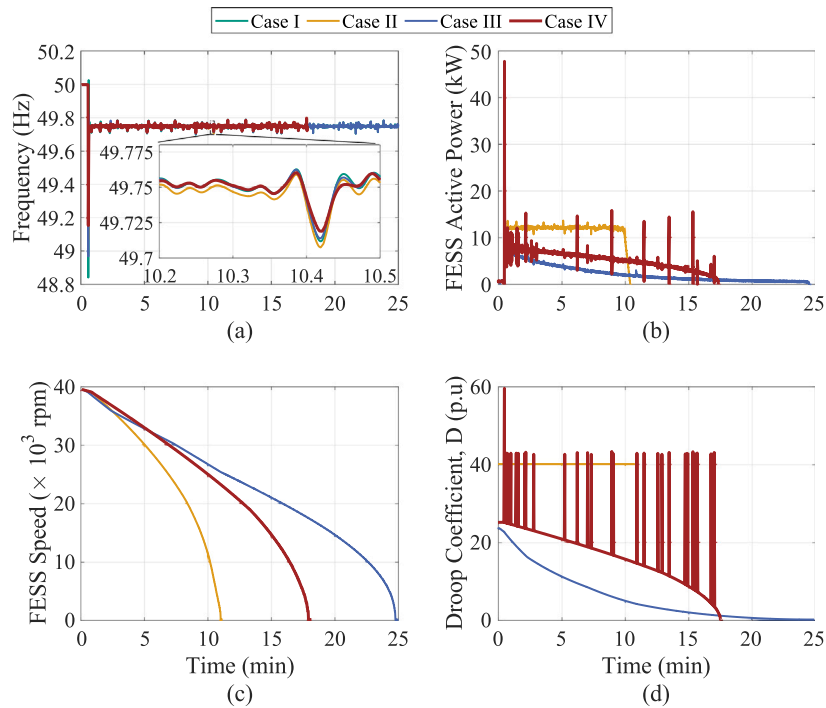
Fig. 7. The results of rapid control prototyping and PHIL simulations for scenario B, long-term operation of the microgrid with intermittent generation. (a) The frequency, (b) the measured active power of the FESS, (c) the rotational speed of the FESS, received using the Ethernet connection and the Modbus protocol, and (d) the variations of the droop coefficient.

The results of the rapid control prototyping and PHIL testing of the 60 kW FESS in this scenario is depicted in Fig. 7. It can be observed from Fig. 7(c) that using the proposed controller, the FESS is emptied much later than the constant droop controller of case II. While the controller of case III, can indeed extend the period of in which the FESS can be used for frequency support services (longer than the proposed control design), it cannot regulate the grid frequency as much as the proposed controller. It can be further noted from Fig. 7(a) that the proposed controller performs better in terms of maintaining the frequency in comparison to the other controllers. From Fig. 7(d), it can be seen that with the start of each change in the frequency, the proposed controller shortly increases the droop coefficient. This leads to a sudden sharp response from the FESS, as seen in Fig. 7(b), which limits the microgrid frequency deviation. Providing such fast active power jumps are not a concern for a FESS in the long term, but rather it is one of the main applications of this storage technology [3,24]. When the frequency is recovering towards its steady-state value, the droop coefficient is immediately reduced to minimize the contribution of the FESS. Using the proposed controller, during the steady-steady conditions, the droop coefficient is slowly reduced as a function of the SOC of the FESS, extending the time the FESS can be used for frequency support applications, in comparison to the conventional droop control of case II.

4. Conclusion

A FESS is known for its quick response and high power capabilities, which can help maintain the frequency in low-inertia power systems. However, the energy density of this storage technology is still quite limited, resulting in short discharge times. In this work, an adaptive droop control for a FESS is proposed, which aims to maximize the contribution of the FESS during the first instances following a frequency deviation, while limiting its contribution after passing the minimum or maximum point in the frequency. In order to verify the performance of the proposed control design, the controller is implemented on a real 60 kW commercial high-speed FESS using the concept of rapid control

prototyping, and the FESS with the new controller is tested using PHIL simulations in two different scenarios. The experimental results show that the proposed controller performs better than the conventional droop controller and an adaptive droop controller previously suggested in literature, in terms of limiting the maximum frequency deviation during disturbances. Moreover, the proposed controller can extend the period, in which the FESS is available for providing frequency support, by considering the SOC of the FESS in the control design and limiting the contribution of the FESS in the long term.

CRediT authorship contribution statement

Shahab Karrari: Conceptualization, Methodology, Software, Validation, Formal analysis, Investigation, Writing – original draft, Visualization. **Giovanni De Carne:** Resources, Writing – review & editing, Supervision, Project administration, Funding acquisition. **Mathias Noe:** Resources, Supervision, Project administration, Funding acquisition.

Declaration of competing interest

The authors declare that they have no known competing financial interests or personal relationships that could have appeared to influence the work reported in this paper.

Acknowledgments

The authors would like to thank Mr. Christian Lange and Mr. Frank Gröner, for their generous help in conducting the experiments presented in this work at KIT's EnergyLab 2.0.

References

[1] F. Milano, F. Dörfler, G. Hug, D.J. Hill, G. Verbič, Foundations and challenges of low-inertia systems (invited paper), in: 2018 Power Systems Computation Conference, PSCC, Dublin, Ireland, 2018.
[2] ENTSO-E, High Penetration of Power Electronic Interfaced Power Sources and the Potential Contribution of Grid Forming Converters, Tech. Rep., ENTSO-E, Brussels, Belgium, 2019.

[3] N. Miller, D. Lew, R. Piwko, Technology Capabilities for Fast Frequency Response, Tech. Rep., GE Energy Consulting, Schenectady, NY 12345, 2017.

[4] C. Sun, G. Joos, F. Bouffard, Adaptive coordination for power and SoC limiting control of energy storage in an islanded AC microgrid with impact load, IEEE Trans. Power Deliv. 35 (2) (2020) 580–591.

[5] S. Sahoo, S. Mishra, S. Jha, B. Singh, A cooperative adaptive droop based energy management and optimal voltage regulation scheme for DC microgrids, IEEE Trans. Ind. Electron. 67 (4) (2020) 2894–2904.

[6] Y.Z. Zhang, Capacity-based adaptive droop control for battery energy storage operation, in: 2017 IEEE Power & Energy Society General Meeting, Chicago, IL, USA, 2017.

[7] S.I. Gkavanoudis, K.O. Oureilidis, C.S. Demoulias, An adaptive droop control method for balancing the SoC of distributed batteries in AC microgrids, in: 2016 IEEE 17th Workshop on Control and Modeling for Power Electronics, COMPEL, Trondheim, Norway, 2016.

[8] A. Urtasun, P. Sanchis, L. Marroyo, State-of-charge-based droop control for stand-alone AC supply systems with distributed energy storage, Energy Convers. Manage. 106 (2015) 709–720.

[9] X. Lu, K. Sun, J.M. Guerrero, J.C. Vasquez, L. Huang, State-of-charge balance using adaptive droop control for distributed energy storage systems in DC microgrid applications, IEEE Trans. Ind. Electron. 61 (6) (2014) 2804–2815.

[10] R. Sebastián, R. Peña Alzola, Flywheel energy storage systems: Review and simulation for an isolated wind power system, Renew. Sustain. Energy Rev. 16 (9) (2012) 6803–6813.

[11] A. Charalambous, L. Hadjidemetriou, E. Kyriakides, M.M. Polycarpou, A co-ordinated voltage-frequency support scheme for storage systems connected to distribution grids, IEEE Trans. Power Electron. 36 (7) (2021) 8464–8475.

[12] U. Markovic, N. Früh, P. Aristidou, G. Hug, Interval-based adaptive inertia and damping control of a virtual synchronous machine, in: 2019 IEEE Milan PowerTech, Milan, Italy, 2019.

[13] J. Fang, R. Zhang, H. Li, Y. Tang, Frequency derivative-based inertia enhancement by grid-connected power converters with a frequency-locked-loop, IEEE Trans. Smart Grid 10 (5) (2019) 4918–4927.

[14] P. Rodríguez, A. Luna, R.S. Muñoz-Aguilar, I. Etxeberria-Otadui, R. Teodorescu, F. Blaabjerg, A stationary reference frame grid synchronization system for three-phase grid-connected power converters under adverse grid conditions, IEEE Trans. Power Electron. 27 (1) (2012) 99–112.

[15] A. Monti, E. Santi, R. Dougal, M. Riva, Rapid prototyping of digital controls for power electronics, IEEE Trans. Power Electron. 18 (3) (2003) 915–923.

[16] N.B. Lai, A. Tarrasó, G.N. Baltas, L. Marin, P. Rodriguez, External inertia emulation controller for grid-following power converter, IEEE Trans. Ind. Appl. (Early Access) (2021).

[17] S. Karrari, G. De Carne, M. Noe, Model validation of a high-speed flywheel energy storage system using power hardware-in-the-loop testing, J. Energy Storage 43 (2021) 103177.

[18] CIGRE, Technical Brochure 575: Benchmark Systems for Network Integration of Renewable and Distributed Energy Resources, Tech. Rep., CIGRE, Paris, France, 2014.

[19] S. Karrari, H.R. Baghaee, G. De Carne, M. Noe, J. Geisbuesch, Adaptive inertia emulation control for high-speed flywheel energy storage systems, IET Gener. Transm. Distrib. 14 (22) (2020) 5047–5059.

[20] C. Dufour, J. Mahseredjian, J. Bélanger, A combined state-space nodal method for the simulation of power system transients, IEEE Trans. Power Deliv. 26 (2) (2011) 928–935.

[21] A. Benigni, T. Strasser, G. De Carne, M. Liserre, M. Cupelli, A. Monti, Real-time simulation-based testing of modern energy systems: A review and discussion, IEEE Ind. Electron. Mag. 14 (2) (2020) 28–39.

[22] P. Kotsampopoulos, D. Lagos, N. Hatziargyriou, M.O. Faruque, G. Lauss, O. Nzimako, P. Forsyth, M. Steurer, F. Ponci, A. Monti, V. Dinavahi, K. Strunz, A benchmark system for hardware-in-the-loop testing of distributed energy resources, IEEE Power Energy Technol. Syst. J. 5 (3) (2018) 94–103.

[23] S. Karrari, N. Ludwig, V. Hagenmeyer, M. Noe, A method for sizing centralised energy storage systems using standard patterns, in: 2019 IEEE Milan PowerTech, PowerTech 2019, Milan, 2019.

[24] B. Fan, C. Wang, Q. Yang, W. Liu, G. Wang, Performance guaranteed control of flywheel energy storage system for pulsed power load accommodation, IEEE Trans. Power Syst. 33 (4) (2018) 3994–4004.